Electrochemical preparation of vertically aligned, hollow CdSe nanotubes and their p–n junction hybrids with electrodeposited Cu2O

ARTICLE *in* NANOSCALE · JUNE 2014

Impact Factor: 7.39 · DOI: 10.1039/c3nr06917f · Source: PubMed

Nanoscale

PAPER

View Article Online
View Journal | View Issue

Cite this: *Nanoscale*, 2014, **6**, 9148

Electrochemical preparation of vertically aligned, hollow CdSe nanotubes and their p–n junction hybrids with electrodeposited Cu_2O†

Joyashish Debgupta,[a] Ramireddy Devarapalli,[ab] Shakeelur Rahman,[a] Manjusha V. Shelke[ab] and Vijayamohanan K. Pillai*[abc]

Vertically aligned, hollow nanotubes of CdSe are grown on fluorine doped tin oxide (FTO) coated glass substrates by ZnO nanowire template-assisted electrodeposition technique, followed by selective removal of the ZnO core using NH_4OH. A detailed mechanism of nucleation and anisotropic growth kinetics of nanotubes have been studied by a combination of characterization tools such as chronoamperometry, SEM and TEM. Interestingly, "as grown" CdSe nanotubes (CdSe NTs) on FTO coated glass plates behave as n-type semiconductors exhibiting an excellent photo-response (with a generated photocurrent density value of ~470 μA cm^{-2}) while in contact with p-type Cu_2O (p-type semiconductor, grown separately on FTO plates) because of the formation of a n–p heterojunction (type II). The observed photoresponse is 3 times higher than that of a similar device prepared with electrodeposited CdSe films (not nanotubes) and Cu_2O on FTO. This has been attributed to the hollow 1-D nature of CdSe NTs, which provides enhanced inner and outer surface areas for better absorption of light and also assists faster transport of photogenerated charge carriers.

Received 31st December 2013
Accepted 25th May 2014

DOI: 10.1039/c3nr06917f

www.rsc.org/nanoscale

Introduction

One dimensional (1D) nanostructures have attracted a great deal of interest recently due to their unique size and shape dependent properties such as ballistic transport,[1] different longitudinal and transverse electronic and optical properties[2] due to density of state singularities, discrete molecule like behavior along the length or phenomena such as spin-charge separation predicted for a Luttinger liquid.[3–5] More specifically, the discovery of carbon nanotubes (CNTs)[6] has caused a paradigm shift in the field of 1-D nanostructures because of their high surface-to-volume ratio as well as high conductivity, flexibility and tunable electronic structure which allow chemical modifications for specific applications. In this respect, semiconducting nanotubes are more interesting because of a perfect blend of properties like bandgap engineering, stability and processability control by surface functionalization as well as the intrinsic advantage of tubular morphology. These make them promising candidates for applications such as solar cells, catalysis, gas sensing, optoelectronic devices, *etc.*[7,8] Among numerous semiconductors, CdSe is more interesting because of its low bandgap (1.7 eV for bulk CdSe), high absorption cross-section of visible light (C_{abs} = (5.501 × 10^5)a^3 cm^{-1} for absorption at 350 nm, where a is the particle radius in cm)[9] and its tunable and unmatched optical properties with size and shape.[10,11]

So far CdSe nanotubes have been synthesized by various methods such as hot injection synthesis,[12] sonoelectrochemical synthesis[13] or a hydrothermal method,[14] but only very few reports are available with respect to their pure electrochemical synthesis. For example, the electrochemical preparation of vertically aligned, hollow CdSe nanotubes (CdSe NTs) *via* ZnO nanowires (ZnO NWs) as templates.[15] Similarly, a more recent study describes a method to grow template-free 1-D CdSe nanowires through electrodeposition on FTO coated glass substrates.[16] The scarcity of electrodeposition methods in the literature for the preparation of 1-D structures of CdSe can be justified by considering the crystal structure of CdSe and growth kinetics of its planes. The three fastest growing directions of CdSe namely ⟨0001⟩, ⟨01$\bar{1}$0⟩, ⟨2$\bar{1}\bar{1}$0⟩ and ±(0001) are polar surfaces and CdSe grows fast along these directions under applied potentials tending to form particles on conducting substrates rather than the 1-D structure during template free electrodeposition.[16] The latter process of making CdSe NTs is, thus, a better choice and it is more so because the whole process was carried out at room temperature compared to the templateless process (95 °C, DMF solvent). The ZnO core can also be

[a]*Physical and Materials Chemistry Division, National Chemical Laboratory, Pune-411008, India. Fax: +91 20 2590 2636; Tel: +91 20 2590 2566*

[b]*Academy of Scientific and Innovative Research (AcSIR), Anusandhan Bhawan, 2 Rafi Marg, New Delhi-110001, India*

[c]*Central Electrochemical Research Institute, Karaikudi, Tamil Nadu, India-630006. E-mail: vk.pillai@ncl.res.in*

† Electronic supplementary information (ESI) available: See DOI: 10.1039/c3nr06917f

easily removed with NH_4OH giving hollow CdSe NTs.[15] Unfortunately, despite being an important material with promising optoelectronic applications, these CdSe NTs have not been further explored for practical optoelectronic applications. Moreover, no further attempt has been made to understand the electrochemistry of the deposition process, as well as the mechanism of nucleation of these nanotubes.

In the present study, vertically aligned, hollow, transparent CdSe NTs have been prepared on a FTO coated glass substrate *via* ZnO NW template electrodeposition at room temperature and at nearly neutral pH (pH 7.5). Cadmium acetate ($Cd(OAc)_2$), nitrilotriacetic acid (NTA) and sodium selenite (Na_2SeO_3) have been employed for electrodeposition. Detailed analysis of the nucleation process has been studied by electrochemical methods and the so formed NTs have been characterized by SEM, TEM, AFM, Raman spectroscopy, UV-Vis spectroscopy and photoluminescence (PL). An n–p heterojunction diode has been fabricated by combining the CdSe NTs (on FTO glass) with electrodeposited Cu_2O (on separate FTO glass) which has a favorable band alignment (type II) with CdSe energy bands. The device (n-CdSe–p-Cu_2O heterojunction) has been tested for electronic and photoresponse properties. The photoresponse of the device has been measured in the presence of AM 1.5 solar simulated light (100 mW cm^{-2}). The present device shows ~470 μA current increment per unit area (in cm^2) in the presence of light. This photoresponse is considerably larger (~3 times) as compared to its analogous device made with electrodeposited CdSe nanoparticles without ZnO NW template.

Experimental section

Materials synthesis

Cadmium acetate dihydrate [$Cd(OAc)_2 \cdot 2H_2O$] (98%), sodium selenite [Na_2SeO_3] (99%) and nitrilotriacetic acid [NTA] (99%) were purchased from Thomas Baker (AR grade). Sodium hydroxide [NaOH] was procured from Rankem. Zinc nitrate hexahydrate [$Zn(NO_3)_2 \cdot 6H_2O$], hexamine, polyethylenimine (M_w: 800) and ammonium hydroxide [NH_4OH] were obtained from Aldrich and used as received. $CuSO_4 \cdot 5H_2O$ (99.5%) and lactic acid (99%) were purchased from Rankem and Aldrich, respectively. MilliQ water (deionized water, 18 MΩ resistance) was used for the preparation of all the solutions.

ZnO NW arrays were synthesized on a FTO coated glass (7 Ω per square) initially cleaned by sonication in acetone, 2-propanol, and methanol, subsequently rinsed with deionized (DI) water, and finally dried in a nitrogen stream. The FTO coated glass plates were coated with ZnO seed particles (~50 nm size ZnO seeds were prepared by the addition of ethanolic solution of 5.7 mM NaOH to ethanolic 1.4 mM zinc acetate dehydrate solution) by drop casting followed by annealing at 300 °C for 20 min in an inert atmosphere. In order to grow vertically aligned ZnO nanorods on the FTO glass plates, the ZnO seed particle coated FTO glass plates were kept in a glass vial containing the solution comprising 25 mM $Zn(NO_3)_2$, 12.5 mM hexamine, 2 mM polyethylenimine (M_w: 800) and 0.35 M NH_4OH in D.I. water at 90 °C for 3 h. The resulting nanowire arrays were rinsed with D.I. water and sintered at 450 °C in an inert atmosphere for 30 min in order to increase crystallinity.

CdSe nanoparticles were electrodeposited on the FTO coated glass containing ZnO NWs from an aqueous solution of 10 mM $Cd(OAc)_2$, 5 mM Na_2SeO_3 and 50 mM NTA. The pH of the solution was adjusted to 7.5 by drop-wise addition of saturated aq. NaOH solution so that the overall volume does not increase much. A three electrode system was used for the electrodeposition with FTO containing ZnO NWs as the working electrode, and Hg/HgO (0.1 M KOH) and platinum foil as reference and counter electrodes, respectively. A constant potential of −1.2 V (*vs.* Hg/HgO) was applied for 15 min on the working electrode for electrodeposition to get a good quality film of desired thickness. After electrodeposition, the ZnO NWs were selectively removed by dipping them in 25% NH_4OH solution for 1 h. Subsequently, the FTO plate containing CdSe NTs was annealed at 300 °C for 30 min in a N_2 atmosphere and the complete removal of the ZnO NW core was confirmed by recording UV-Vis absorbance at various times of leaching. After 1 h, no ZnO feature was observed in the UV-Vis spectra. Finally, EDAX data also confirmed the absence of ZnO after 1 h.

A Cu_2O nanoparticle film was also electrodeposited on FTO glass from a mixture of 20 mM $CuSO_4$ and 1 M lactic acid aq. solution according to the literature.[17] The pH of the solution was adjusted to 7.5 by drop-wise addition of saturated NaOH solution. A similar set up (except for the working electrode which is clean FTO here) was used for Cu_2O deposition using a constant potential of −0.55 V (*vs.* Hg/HgO) for 2 min for the deposition. The deposit was subsequently annealed at 150 °C in an inert atmosphere.

Characterization

Powder X-ray diffraction patterns were recorded on a Phillips PANalytical diffractometer with CuKα radiation ($\lambda = 1.5406$ Å), with a scan speed of 2° min^{-1} and a step size of 0.02° in 2θ. All Raman spectroscopy measurements were carried out at room temperature on an HR 800 Raman spectrophotometer (Jobin Yvon HORIBA, France) using monochromatic radiation emitted by a He–Ne laser (632 nm), operating at 20 mW. The experiment was repeated several times and at several places to verify the consistency of the spectra. Transmission electron microscopy was carried out using a JEOL JEM 1200 EX operating at an accelerating voltage of 200 kV with a resolution of not less than 3–4 nm. UV-Vis spectra were recorded using a Carry Win 50 (Agilent Tech.). Steady-state photoluminescence emission was carried out using a Fluorolog HORIBA Jobin Yvon fluorescence spectrophotometer. Measurements were carried out at 22.5° in front-face films (in solid state). The morphological analysis of the materials as well as EDAX analyses was performed using a Quanta FEI 200-3D scanning electron microscope (SEM) equipped with a Phoenix energy dispersive X-ray (EDX) analyzer. All electrochemical measurements were carried out by sweeping the potential at 20 mV s^{-1} using a BioLogic SP300 potentiostat both in the dark as well as in the presence of 1.5 AM solar simulated light (100 mW cm^{-2}). A Newport IPCE measurement setup was used for getting responsivity at various wavelengths

coupled to a Keithley 2400 SMU for electrical measurement *in situ*. Photoconductance was measured using LEDs of different wavelengths. All the electrical measurements were carried out inside a dark room under ambient conditions.

Results and discussion

Fig. 1 shows a simple and overall process of CdSe NT formation. In order to understand the nucleation and growth process during the CdSe electrodeposition, cyclic voltammetry (CV) and chronoamperometry (CA) were performed. Accordingly, Fig. S3† is a typical voltammogram recorded in a mixture of $Cd(OAc)_2$, Na_2SeO_3 and NTA using FTO (with no ZnO) as the working electrode at a scan rate of 20 mV s^{-1}. C1 and C2 (Fig. S3†) are the corresponding reduction peaks according to eqn (1) and (2), respectively. Similarly, Fig. 2(a) shows a typical voltammogram of CdSe electrodeposition from solution using ZnO NW coated FTO glass as the working electrode. This CV shows two cathodic humps (C1 and C2) for the electro reduction of Na_2SeO_3, but no oxidation peak corresponding to this is observed during the anodic scan. The two reduction peaks are not well resolved in this case because the high iR drop due to ZnO can mask the peaks. C1 corresponds to the reduction of SeO_3^{2-} into Se(0) metal and C2 is due to the reduction of Se(0) to form Se^{2-}. The absence of any oxidation peak in the anodic scan is probably due to the formation of CdSe by reacting with the Cd^{2+} present in the solution (actually a complex of Cd^{2+} and NTA) and so the reduced species Se^{2-} is consumed before oxidation. NTA actually shifts the reduction potential of Cd^{2+} towards much negative potential by forming a chelate and so Cd^{2+} reduction is not observed within the present electrochemical window. The reaction may be summarized as follows.

$$SeO_3^{2-} + 3H_2O + 4e^- = Se^0 + 6OH^-,\ E^0 = -0.36\ \text{V}\ \textit{vs.}\ \text{NHE} \quad (1)$$

$$Se^0 + 2e^- = Se^{2-},\ E^0 = -0.92\ \text{V}\ \textit{vs.}\ \text{NHE} \quad (2)$$

$$Cd^{2+} + Se^{2-} = CdSe\downarrow \quad (3)$$

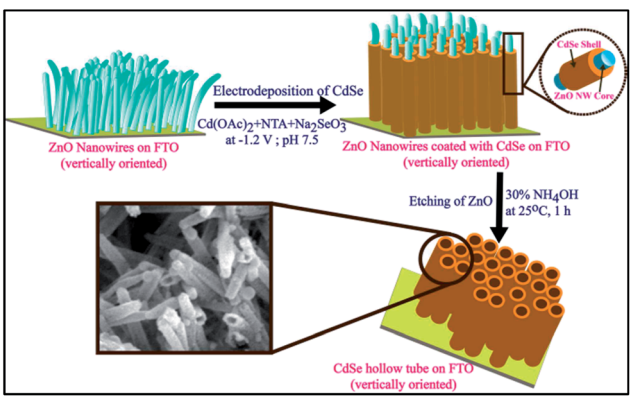

Fig. 1 Controlled electrochemical synthesis of vertically aligned, hollow CdSe nanotubes on FTO-glass by ZnO NW templating and subsequent ZnO core dissolution with ammonium hydroxide.

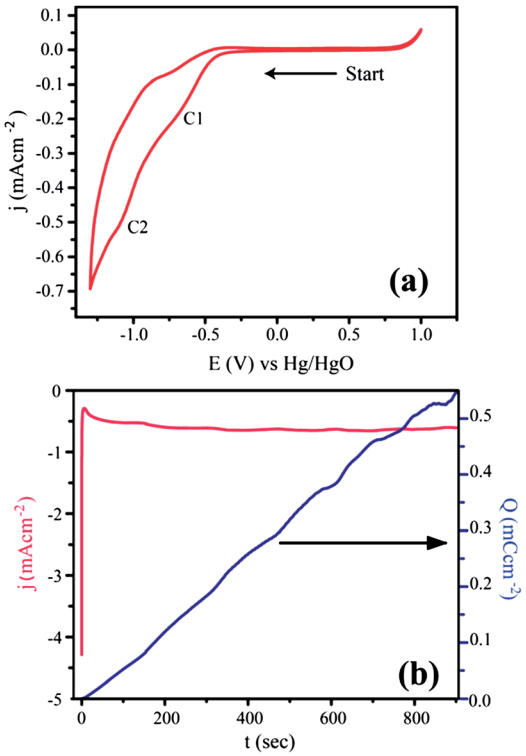

Fig. 2 (a) Cyclic voltammogram recorded using the ZnO NW–FTO working electrode in a solution containing $Cd(OAc)_2$, Na_2SeO_3 and NTA; (b) chronoamperogram (pink) and total charge passed (blue) during the deposition process.

Overall reaction is

$$SeO_3^{2-} + Cd^{2+} + 3H_2O + 6e^- = CdSe\downarrow + 6OH^- \quad (4)$$

The electrochemical reactions are similar to that observed for CdTe electrodeposition on ZnO NWs.[18] ZnO NWs generally make the surface hydrophobic because of their surface roughness. Hence, the ZnO NW layer imposes diffusion limitation to the redox species in the solution towards the FTO electrode and the reduction peak becomes broad, especially when the ZnO layer is compact and the thickness is more (more than 2 μm), the solution cannot penetrate through the pinholes and so the CV feature is not clearly visible (Fig. 2(a), the reduction peak is not very prominent). On the other hand, the ZnO surface is highly insulating so that peaks are broadened. In this case we do not observe any deposition at the potential selected. Fig. 2(b) is the corresponding chronoamperogram of CdSe electrodeposition on ZnO NWs deposited for 15 min. It shows an increase in current until a maximum is reached, followed by a decrease in current and then saturation up to 900 s (15 min). The peak below 12 s in the chronoamperogram is due to nucleation and subsequent merging of individual nucleus. At −1.2 V, Se^{2-} is generated, which then reacts with Cd^{2+} to form CdSe and hence nucleation sets in. After that again the current decreases. The plateau region is the initial growth period and the peak indicates the region where nucleation occurs. To further explore the

nucleation mechanism, we have further studied the chronoamperogram in the short time region (up to 100 s).[19]

Accordingly, Fig. 2(a) shows the current–time behavior during the deposition in the short time region. To understand the mechanism from this plot, we can divide the whole plot into three distinct regions.

Region-I: very short region (within 4–5 s). In this region the current is inversely proportional to the square root of time and thus indicates that the process is under diffusion controlled. Such a dependency is in accordance with Cottrell behaviour and is indicative of instantaneous nucleation where all the nuclei form at the same time.[19]

Region-II: intermediate region where a quadratic relationship between normalized current (i/i_m) and normalized time (t/t_m) is observed where i and i_m indicate current and maximum current at the peak, respectively. Similarly, t and t_m represent time and the time when maximum current is reached, respectively. Following two equations (by Scharifker and Hills) are often used as a diagnostic test for the type of nucleation during electrodeposition.[19]

$$\left(\frac{i}{i_m}\right)^2 = \frac{1.9542}{\frac{t}{t_m}}\left\{1-\exp\left[-1.2564\left(\frac{t}{t_m}\right)\right]\right\}^2 \quad (5)$$

$$\left(\frac{i}{i_m}\right)^2 = \frac{1.2254}{\frac{t}{t_m}}\left\{1-\exp\left[-2.3367\left(\frac{t}{t_m}\right)^2\right]\right\}^2 \quad (6)$$

where eqn (5) and (6) are for instantaneous and for progressive nucleation processes, respectively. Here, i_m is the maximum current (or peak current) in the chronoamperogram and t_m is the time pertaining to that maximum current.

In the present case the normalized current–normalized time relationship follows the behavior known for an instantaneous nucleation mechanism. Fig. 3 clearly demonstrates that in the short-time region the kinetics of nucleation follows the instantaneous pathway rather than the progressive one although it deviates when $t > t_m$. Both regions I and II support this mechanism. Actually, the nucleation starts at the FTO base (FTO glass coated with ZnO NWs) and progressive growth occurs along the walls of ZnO NWs with time.

Region-III: the nuclei grow further along the walls of ZnO NWs facilitating an increase in thickness of NWs with time as reported previously.[15]

In this deposition process, pH plays a crucial role and accordingly, we have found pH 7.5 to be optimum for smooth deposition. Above or below this pH no deposition occurs and instead ZnO NWs dissolve out. This might be due to the fact that the point of zero charge (PZC) of ZnO is at ~pH 8.[20] This might also be explained due to the pH sensitivity of the SeO_3^{2-} reduction in alkaline medium where OH^- is generated during the selenite reduction to selenium (eqn (1)). Temperature also has a profound effect on the rate of deposition. We have, however, carried out all the deposition process only at room temperature (30 °C) in order to have a meaningful comparison. CdSe deposition was also observed below −1.2 V (up to −0.96 V *vs.* Hg/HgO, *i.e.*, the onset of the second reduction peak C2 in the voltammogram) although the rate and quality of deposition are poorer than those observed at −1.2 V. With an increase in deposition time, the outer diameter of CdSe NTs increased significantly as has been reported previously,[15] despite no enhancement of length.

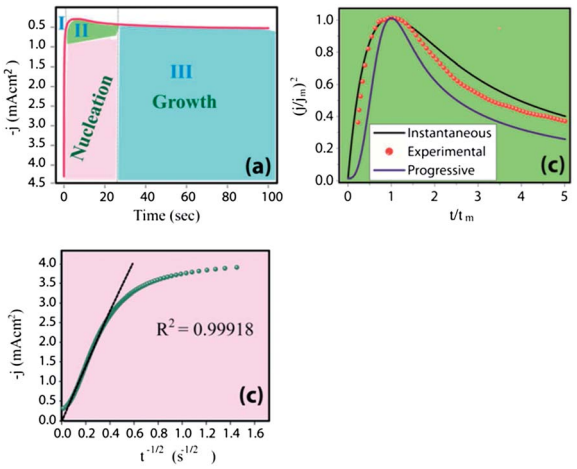

Fig. 3 (a) Chronoamperogram during CdSe deposition at −1.2 V *vs.* Hg/HgO (within 100 s); (b) dimensionless i–t transient for nucleation of CdSe on ZnO NWs and corresponding theoretical plots for instantaneous and progressive nucleations; (c) current density *vs.* $t^{-1/2}$ during the initial stage of deposition on ZnO NWs (within 4–5 s) showing the process under controlled diffusion. Plots (b) and (c) suggest an instantaneous nucleation mechanism.

Scanning electron micrographs of ZnO NWs as well as CdSe NTs on FTO coated glass are shown in Fig. 4(a) and (b), respectively. All ZnO NWs are ~2.5 μm long and have ~150–170 nm diameter and reveal vertical alignment with respect to the substrate (FTO coated glass) plane and the approximate density of the as grown nanowires is $\sim 3 \times 10^9$ cm^{-2}. However, after the CdSe deposition, the diameter of each NW increases and more significantly, the surface becomes rough (Fig. 4(c) and (d)) indicating the successful deposition on the walls of ZnO. In comparison after leaching the ZnO NW core with 25% NH_4OH for 1 h, images clearly reveal the presence of CdSe hollow tubes as displayed in Fig. 4(e) and (f), respectively. These tubes reveal the same length as that of the ZnO NWs and EDAX analysis confirms the presence of only CdSe (1 : 1.5 ratio). More important is the conspicuous absence of ZnO thus ensuring perhaps the near-complete removal of the ZnO core. A closer look at the tips of the so formed CdSe NTs reveals their hexagonal morphology which is similar to that seen in the case of ZnO NW tips. This observation thus implies that the growth of CdSe occurs along the walls of ZnO NWs and hence the morphology is retained even after the removal of template ZnO. The ZnO NWs look thicker and rougher after CdSe electrodeposition (Fig. 4(d)) than the pristine NWs. In order to get more insight into the structure, we have carried out TEM (transmission electron microscopy) analysis of the CdSe NTs. Accordingly, Fig. 5 depicts the high resolution TEM images of the as grown ZnO NWs and annealed CdSe NTs. The diameter of a single ZnO nanowire is ~60–70 nm (Fig. 5(a)), but the diameter is found to

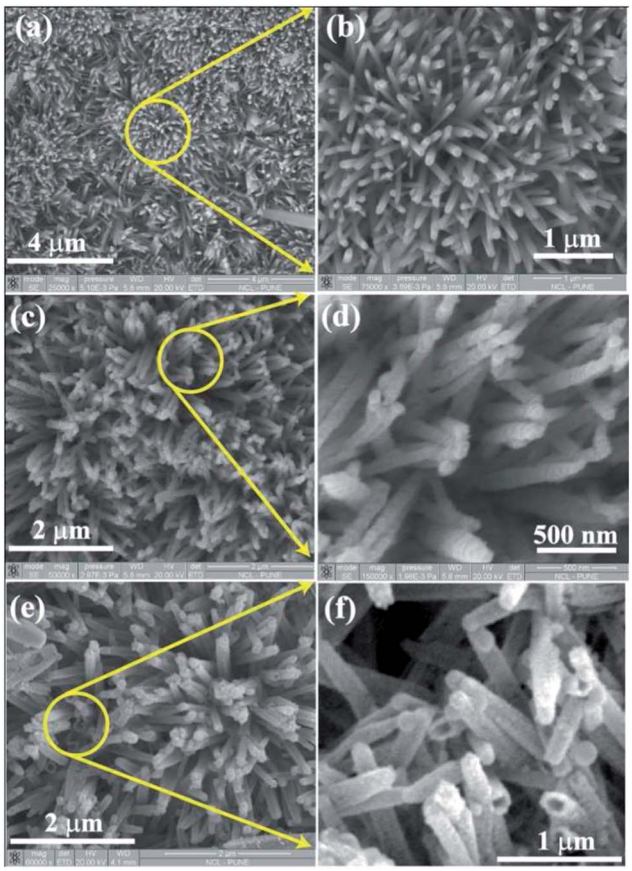

Fig. 4 Scanning electron micrographs of (a) top view of ZnO NWs; (b) ZnO NWs with enlarged portion; (c) ZnO NWs covered with electrodeposited CdSe (top view); (d) enlarged view of ZnO NWs covered with CdSe; (e) CdSe nanotubes (CdSe NTs) after leaching out the ZnO NW core (top view) and (f) enlarged view of the CdSe nanotubes. The tip of CdSe NTs retains the hexagonal shape (40–50 nm diameter and 2.5 μm in length) of the ZnO NW tip and thereby gives evidence for nanowire templating.

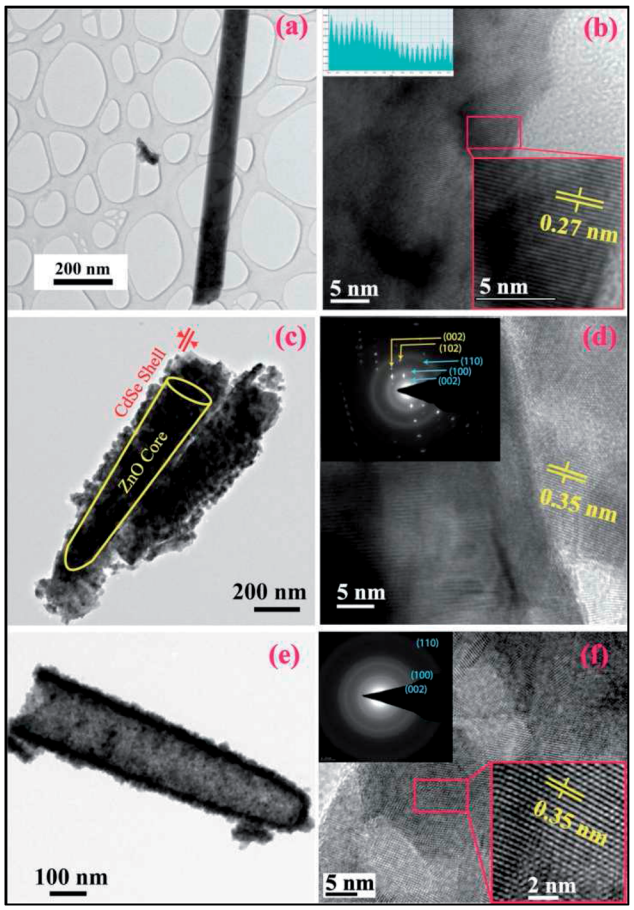

Fig. 5 High resolution transmission electron micrographs of CdSe nanotubes (CdSe NTs) grown vertically by electrochemical deposition using ZnO NWs as the template. (a) A single ZnO nanowire and (b) its high magnification image revealing its atomic planes (inverse FFT pattern and an enlarged portion of the atomic planes are shown in the inset); (c) ZnO NW core and CdSe shell (before leaching); (d) its high resolution image showing atomic planes of both CdSe and ZnO; the inset shows the selected area diffraction (SAED) pattern; (e) a single CdSe nanotube showing the absence of the ZnO core and (f) high resolution CdSe NTs showing atomic planes, selected area diffraction pattern (SAED) of the CdSe NT showing (002) and (100) planes to be exposed preferentially, and lattice planes (the inset is the enlarged portion of the atomic planes) with a *d*-spacing of 0.35 Å indicating the primitive hexagonal crystal structure of the nanotubes.

increase (~242 nm) after electrodeposition of CdSe on ZnO NWs which is clearly seen in Fig. 5(c). On the other hand, the diameter of the nanotubes does not change after the dissolution of the ZnO NW core (Fig. 5(e)). Moreover, a comparative study of high resolution images of ZnO NWs, CdSe deposited ZnO NWs and CdSe NTs (Fig. 5(b), (d) and (f) respectively) reveals the presence of the CdSe shell on the ZnO core, because the lattice fringe patterns are different in three different cases. Indexing of the spots for ZnO reveals that (002) and (102) planes are mostly exposed. For example, in Fig. 5(b), the outer wall of the nanowires shows characteristic *d*-spacings of 2.7 Å for ZnO, whereas Fig. 5(d) shows two different types of *d*-spacings: the outer portion (edge) mainly comprises CdSe (3.5 Å) but the center region has two types of lattice fringes due to the presence of both CdSe and ZnO. Thus TEM analysis proves the critical role of ZnO NWs as the template for the growth of hollow CdSe nanotubes. As can be seen from Fig. 5(e) and (f), the surface of each CdSe NT is granular and consists of CdSe nanoparticles of size 8–10 nm (Fig. 5(f)) as illustrated in the enlarged view of Fig. 5(e).

These nanoparticles are deposited on the walls of ZnO NWs and linked together to form a tubular morphology. These particles are interconnected by strong cohesive forces as they do not get separated easily even upon ultrasonication, which is especially relevant for the sample after annealing at 300 °C in a N_2 atmosphere. Fig. 5(f) is a representative selected area diffraction pattern (SAED) of the CdSe NTs showing (002), (100), and (110) planes.

The sharp nature of the diffraction rings is indicative of the crystalline nature of the NTs and an assignment of the rings shows that the (002) plane is more intense than the (110) plane. This thus implies that the growth of CdSe NTs is along the ⟨002⟩ direction (*c*-axis). The *d*-spacing obtained both from SAED as well as lattice fringes (3.5 Å) is in good agreement with the

primitive hexagonal phase formation (JCPDS card no. 77-0046) and matches well with those obtained previously.[21] The core–shell nature of ZnO NW–CdSe is also evident from the SAED pattern. Its high magnification image (Fig. 5(d)), revealing its atomic planes, shows the ZnO NW core and CdSe shell (before leaching) and the inset shows the selected area diffraction (SAED) pattern for the same. Fig. 5(e) is the representative TEM image of a single CdSe nanotube showing the absence of the ZnO core and Fig. 5(f) is the high resolution image of CdSe NTs showing atomic planes. The selected area diffraction pattern (SAED) of the CdSe NTs shows (002) and (110) planes to be exposed preferentially. The lattice plane with a *d*-spacing of 3.5 Å, indicates the primitive hexagonal crystal structure of the nanotubes. Selected area diffraction (SAED) patterns of ZnO NWs and CdSe–ZnO NW hybrids as well as CdSe NTs are shown in the inset of Fig. 5(b), (d) and (f), respectively. For the ZnO–CdSe system (before leaching the ZnO), two different types of SAED spots are observed (Fig. 5(d)), whereas in the case of CdSe NTs (Fig. 5(f)), only the ring pattern is observed. This is because of the presence of both ZnO and CdSe particles after electrodeposition and thus confirms the core–shell nature of the hybrids. However, after leaching out the ZnO core, the characteristic dot SAED pattern disappears and only the ring pattern of CdSe is observed. This is also an indication of complete removal of ZnO.

Fig. 6 shows the micro-Raman spectrum of CdSe nanotubes, recorded using a 632.8 nm laser line with a 50× objective lens. For comparison, the Raman spectrum of electrodeposited CdSe nanoparticles (CdSe NPs on FTO without any ZnO NW template) is also displayed along with that of CdSe NTs. Both the spectra show characteristic longitudinal optical phonon (LO) modes arising due to Se–Cd–Se symmetric vibration[22] at 205 cm^{-1} for CdSe NPs and at 208 cm^{-1} for CdSe NTs. The appearance of a peak below 210 cm^{-1} confirms that CdSe is in the nanosize range because the same peak comes at 210 cm^{-1} for bulk CdSe.

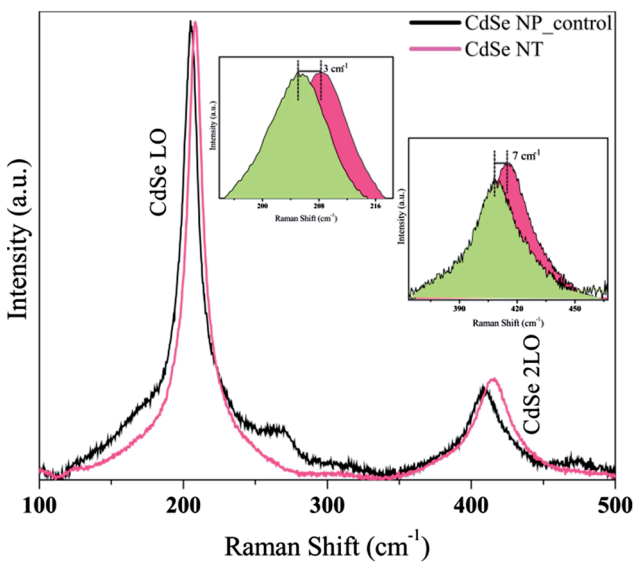

Fig. 6 A comparison of the micro-Raman spectra of CdSe nanoparticles (black line) with those of CdSe nanotubes (red line). All the measurements were taken using a 632.8 nm He–Ne laser line (20 mW source energy) with a 50× objective lens. No density filter was used for the measurement. Insets are the enlarged portion of the LO (200–214 cm^{-1}) and 2LO (360–450 cm^{-1}) bands, respectively. Both the bands shift bathochromically in the case of nanotubes, although the amount of shift is more for the 2LO band.

The second order bands (2LO) have also appeared in the spectra at 408 for CdSe NPs and at 415 cm^{-1} in the case of CdSe NTs. This band originates due to a double resonance process during the Raman scattering. Interestingly, both positions of LO and 2LO peaks of CdSe NTs have been shifted to a higher wavenumber (or higher energy) by 3 and 7 cm^{-1} respectively compared to that of CdSe NPs. Interestingly, the full width at half maximum (FWHM) of the LO peak also decreases slightly in the case of CdSe NTs compared to that of CdSe NPs. This ostensibly suggests the quantum confinement effect, since both the LO and 2LO peak frequencies show a blue shift. However, a careful inspection of the TEM structures suggests that the nanoparticles, consisting the NTs, are of 8–10 nm in size which is far beyond the strong confinement region for CdSe (exciton Bohr radius is 5.4 nm for bulk CdSe).[23]

Hence quantum confinement is not expected to explicitly contribute to the shift of the phonon peaks. A more appropriate explanation for the shift might be the presence of surface traps. It is well known that CdSe nanoparticles have surface defects (or traps) on their surface due to a high surface-to-volume ratio and the extent of defect increases when the nanoparticles assemble into a quasi 1D structure like nanotubes.[24] So the net surface defect content is significantly higher in the case of CdSe NTs than that for CdSe NPs. This higher defect content may be responsible for shifting the fundamental phonon modes of CdSe NPs to higher energy.[24]

Cu_2O is a well-known p-type material (since the majority carrier is a hole due to naturally forming cation vacancies and not electrons) with a bandgap of 2.2 eV[25] and its valence and conduction bands (VB and CB, respectively) are at 1.30 and −0.70 V (*vs.* NHE), respectively. These bands are well aligned with the VB and CB of CdSe (1.32 and −0.59 V *vs.* NHE).[26] Hence, a remarkable combination of both these can in principle give rise to a significant heterojunction (Fig. 7(a)) which can show good optoelectronic properties. FTO glass containing CdSe NTs was then brought into intimate contact with the FTO glass containing Cu_2O in order to establish the n–p hetero-junction. Here, CdSe has a band-gap of 1.7 eV (Fig. S11†) and that of Cu_2O is 2.4 eV (Fig. S10†). The device shows rectifying behavior in the dark with a rectification ratio ($I_{forward}/I_{reverse}$) of 3 at a bias of 0.6 V, indicating the formation of a p–n junction diode. The "turn on" voltage is 0.13 V and the reverse leakage current value is 7×10^{-5} A at −1 V (Fig. 7(b)).[27] In order to see the effect of CdSe NT–FTO and Cu_2O–FTO junctions on the *I–V* characteristics of the n–p heterojunction, *I–V* measurement was carried out for the respective junctions in a similar flip-chip method. Fig. S8 and S9† show the *I–V* characteristics of CdSe NT–FTO and Cu_2O–FTO junctions, respectively. The Cu_2O–FTO junction shows ohmic behaviour at very low voltage (within ±0.04 V), but changes to the Schottky type at voltage larger than this threshold voltage. On the other hand, the CdSe NT–FTO junction shows ohmic behavior up to ~0.6 V. The absorption

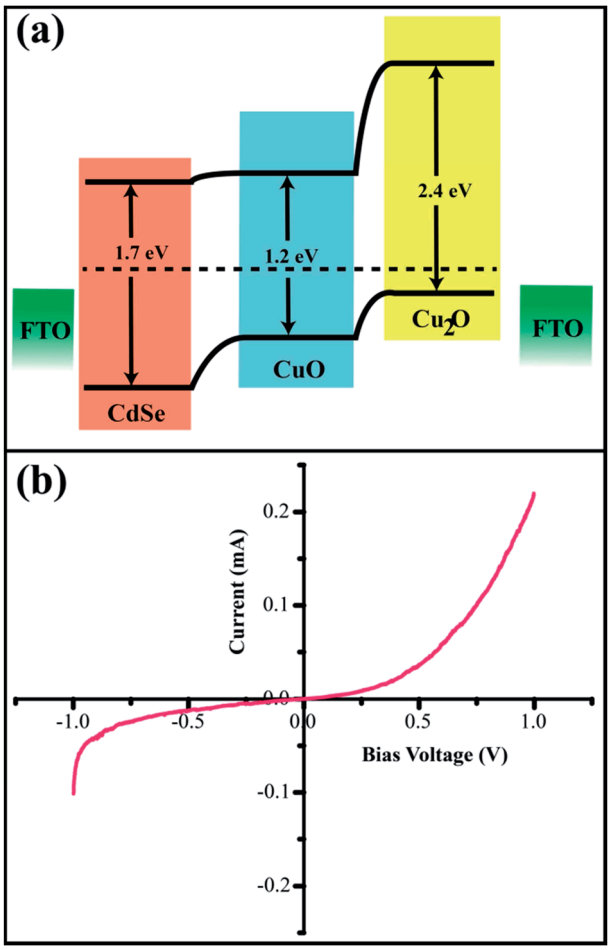

Fig. 7 (a) Band alignment diagram of CdSe and Cu_2O. Type II band alignment is responsible for photoresponse and (b) current–voltage (*I–V*) characteristics of the n–p heterojunction device comprising CdSe NTs and Cu_2O (device area 1 cm^2). The plot shows the rectifying nature of the device.

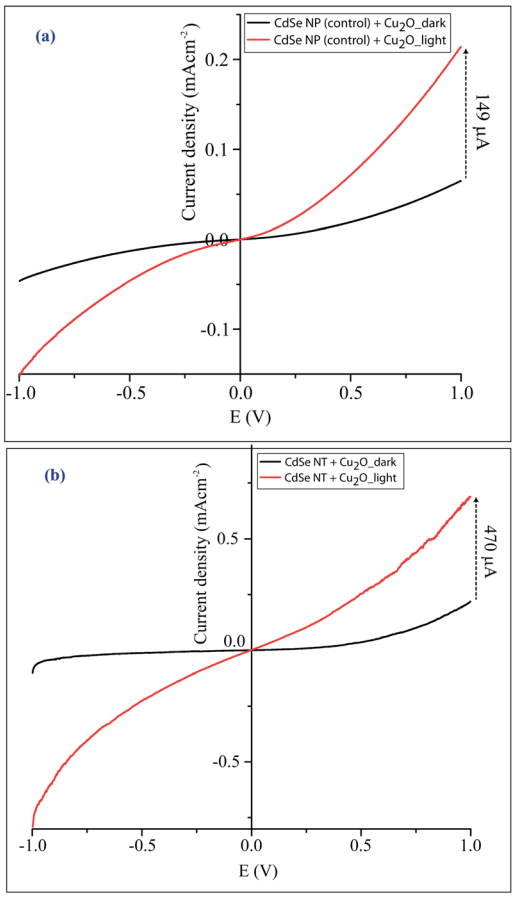

Fig. 8 Current–voltage (*I–V*) characteristics of CdSe–Cu_2O heterojunction devices (n–p junction) in the dark (black) and under AM 1.5 solar simulated light (*i.e.*, 100 mW cm^{-2}) (red); (a) corresponds to the device with CdSe nanoparticles (NPs)–Cu_2O and (b) with CdSe NTs–Cu_2O.

spectrum of electrodeposited Cu_2O (Fig. S10†) shows the presence of a very small amount of CuO formed due to aerial oxidation on the surface of Cu_2O. But the presence of CuO (a p-type Mott insulator) does not affect the electron transfer from p-type Cu_2O because the VB and CB of the latter are properly aligned with CdSe (Fig. 7(a)) so as to allow electron transfer from p-type Cu_2O to n-type CdSe NTs on excitation with light.

The device shows a stronger photoresponse when compared with that obtained for CdSe NPs as an n-type material. Fig. 8 shows the photoresponse of the so formed device in the presence of AM 1.5 solar simulated light. For CdSe NTs, the increment in current on irradiation is ~470 μA whereas for a similar device with CdSe NPs gives ~149 μA increment in the presence of light when a forward bias of 1 V was applied. The much larger photoresponse (~3.2 times) of the device consisting of CdSe NTs obviously comes from the quasi 1D nanostructures, which efficiently generates excitons and the 1D structure of CdSe provides an expressway for carrying the electrons to the FTO coated glass which act as the current collector. Thus the device can be a promising candidate for harvesting light energy.

In order to understand the effect of different light on the photoresponse of the n–p heterojunction device, responsivity of the device has been studied at various wavelengths of light using a monochromatic light source. Responsivity has been calculated by dividing photocurrent flowing through the device with power of the incident light.[28] Accordingly, Fig. 9 shows the normalized responsivity plot as a function of wavelength of incident light. The plot gives a maximum at 700 nm with a small hump between 500 and 600 nm. The highest responsivity in the near IR region can be attributed to the absorption of light by CdSe NTs (λ_{max} = 662 nm, Fig. S11†) which absorb strongly in this region due to low bandgap as well as higher inner and outer accessible surface areas for incident light. CdSe absorbs a higher amount of light and generates a large number of excitons which dissociates at the CdSe–Cu_2O junction thereby giving higher photocurrent at 700 nm. On the other hand, Cu_2O absorbs in the region of 350 to 580 nm in the spectrum (Fig. S10†). Hence, the responsivity shows a small hump in the region from 500 to 600 nm indicating that Cu_2O absorption predominates in generating excitons and photocurrent as a

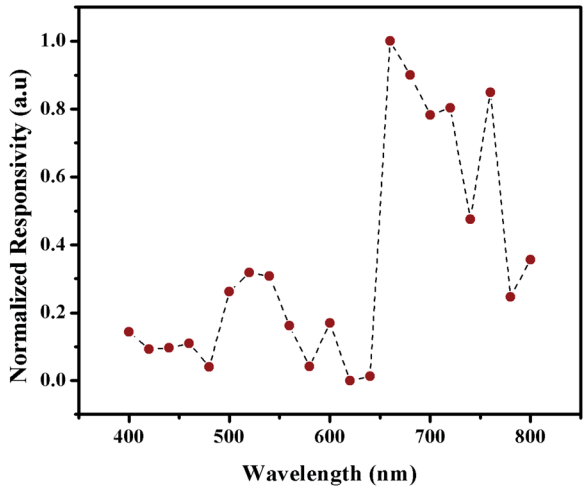

Fig. 9 Normalized responsivity as a function of wavelength. The device was illuminated from the Cu_2O side.

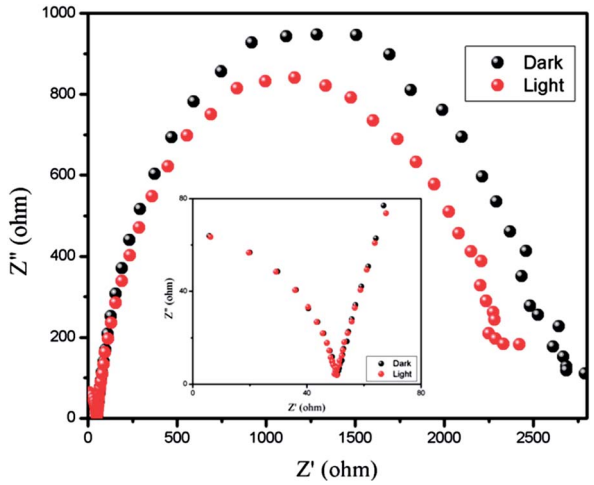

Fig. 10 Nyquist plot for the CdSe NT–Cu_2O n–p heterojunction device in the dark (black) and under AM 1.5 solar simulated light (red). The inset is the high frequency semicircle which does not change even on exposure to light and therefore is less important. The low frequency semicircle however decreases in the presence of light and thus related to the generation and recombination of charge carriers. The diameter of the second semicircle (low frequency) indicates charge transfer resistance which is reduced upon illumination.

consequence. But, the Cu_2O film has a lower surface area for absorption of light as compared to CdSe NTs. The responsivity in this region is, therefore, not as high as in the case of CdSe NTs at higher wavelength of light. Moreover, the device has been illuminated from the Cu_2O side which is a higher bandgap (2.4 eV) material than CdSe. Light of wavelengths less than 600 nm, therefore, cannot pass through the Cu_2O film to reach CdSe NTs and so CdSe NTs do not contribute much to the photoconductivity of the device below 600 nm. Similarly, the photons having wavelengths greater than 600 nm are absorbed mostly by CdSe NTs and not by Cu_2O causing a higher photoresponse. Cu_2O in combination with CdSe NTs thus acts as a visible light sensitive photodetector which can work at any wavelength ranging from 400 to 800 nm.

Impedance measurement has been performed to understand the junction as well as to get the electron transport properties of the junction. The frequency range used for the measurement is 1 MHz to 0.1 Hz and with an AC amplitude of 10 mV. Impedance measurement was carried out both in the dark as well as in the presence of AM 1.5 solar simulated light (100 mW cm^{-2}). Accordingly, Fig. 10 presents the Nyquist plot for the device in the dark and under light. The low frequency semicircle decreases (319 Ω) upon illumination. This indicates probably the reduced charge transfer resistance at the interface. The VB and CB of CdSe are well aligned with those of Cu_2O and hence the photogenerated minority carriers (electron) in Cu_2O can be easily transferred to the CB of CdSe NTs. At the same time the hole can migrate from the VB of CdSe to the VB of Cu_2O (Fig. 7(a)). This thereby reduces the probability of recombination and hence the decrease in charge transfer resistance as well as improved photocurrent generation in the case of CdSe NTs and Cu_2O heterojunction.

Thus from the above data we see a successful preparation of vertically aligned, hollow CdSe NTs on a conducting glass substrate (FTO coated glass) by ZnO NW templating. SEM and TEM provide distinct evidence for the hollow structure and more significantly CdSe NTs can form a proper n–p heterojunction diode with p-type Cu_2O, deposited electrochemically, in a current perpendicular to plane (CPP) geometry. The diode shows a good photoresponse as compared to those of devices made of electrodeposited films of CdSe NPs without the ZnO NW template.

Nevertheless, the present study is carried out only with electrodeposited Cu_2O and no shape and size selective activity has been investigated. Experiments are currently going on to explore these aspects. Moreover, the temperature has a profound effect on the performance of n–p diodes because thermal energy also promotes diffusion charge carriers across the interface. The light intensity as well as the interface structure also affects the photoconductivity of such devices. However, these experiments require much time and sophisticated instrumentation which are out of the scope of the present study.

Conclusion

In conclusion, vertically aligned quasi 1-D CdSe NTs with a hollow inner core have been grown on transparent conducting glass (FTO-glass) substrates using a simple electrochemical deposition technique–zinc oxide nanowires, grown on FTO-glass, act as the structure directing template for the growth of these nanotubes. The deposition has been found to depend strongly on the pH, concentration of species, applying voltage and also temperature. The nucleation mechanism of CdSe deposition has been shown to follow an instantaneous pathway. Moreover, these nanotubes are found to form a rectifying n–p heterojunction diode with p-type Cu_2O deposited electrochemically. The heterojunction shows a strong photoresponse (~470 μA cm^{-2} current density increment with 100 mW cm^{-2}

light) and the photosensitivity is better (~3 times more) than that in the case of an electrodeposited CdSe nanoparticle film. Thus the present study is expected to be a general platform for the preparation of devices applied for solar cells, photodetectors and other optoelectronic devices.

Acknowledgements

JD sincerely acknowledges University Grants Commission and CSIR, India for fellowship and Dr K. Sreekumar for kind help. We are also thankful to Dr S. Pal, Director, CSIR-NCL for support and infrastructure. We thank Ketan, Pandiaraj, and Shraviya for SEM and TEM analyses. We also acknowledge Dr C. S. Gopinath and Kanak Roy from the Center of Excellence on Surface Science (CoES), CSIR-NCL for XPS analysis.

Notes and references

1 S. Ciraci, A. Buldum and I. P. Batra, *J. Phys.: Condens. Matter*, 2001, **13**, R537.
2 S. Link and M. A. El-Sayed, *J. Phys. Chem. B*, 1999, **103**, 8410.
3 J. Voit, *Rep. Prog. Phys.*, 1995, **58**, 977.
4 C. Kane, L. Balents and M. P. Fisher, *Phys. Rev. Lett.*, 1997, **79**, 5086.
5 C. M. Lieber, *Solid State Commun.*, 1998, **107**, 607.
6 S. Iijima, *Nature*, 1991, **354**, 56.
7 C. Rao and A. Govindaraj, *RSC Nanosc. and Nanotech. Series*, RSC Publishing, Cambridge, UK, 2005.
8 (*a*) K. Zhu, N. R. Neale, A. Miedaner and A. J. Frank, *Nano Lett.*, 2007, **7**, 69; (*b*) K. Shankar, G. K. Mor, H. E. Prakasam, S. Yoriya, M. Paulose, O. K. Varghese and C. A. Grimes, *Nanotechnology*, 2007, **18**, 065707; (*c*) P. Roy, D. Kim, K. Lee, E. Spiecker and P. Schmuki, *Nanoscale*, 2010, **2**, 45; (*d*) A. B. Martinson, M. S. Goes, F. Fabregat-Santiago, J. Bisquert, M. J. Pellin and J. T. Hupp, *J. Phys. Chem. A*, 2009, **113**, 4015; (*e*) Q. Zhang, C. S. Dandeneau, X. Zhou and G. Cao, *Adv. Mater.*, 2009, **21**, 4087.
9 C. Leatherdale, W.-K. Woo, F. Mikulec and M. Bawendi, *J. Phys. Chem. B*, 2002, **106**, 7619.
10 (*a*) D. Norris and M. Bawendi, *Phys. Rev. B: Condens. Matter Mater. Phys.*, 1996, **53**, 16338; (*b*) W. K. Leutwyler, S. L. Bürgi and H. Burgl, *Science*, 1996, **271**, 933.
11 (*a*) L.-s. Li, J. Hu, W. Yang and A. P. Alivisatos, *Nano Lett.*, 2001, **1**, 349; (*b*) M. B. Mohamed, C. Burda and M. A. El-Sayed, *Nano Lett.*, 2001, **1**, 589.
12 C. Rao, A. Govindaraj, F. L. Deepak, N. Gunari and M. Nath, *Appl. Phys. Lett.*, 2001, **78**, 1853.
13 Q. Shen, L. Jiang, J. Miao, W. Hou and J.-J. Zhu, *Chem. Commun.*, 2008, **14**, 1683.
14 G. Nagaraju and G. T. Chandrappa, *J. Mater. Sci. Technol.*, 2012, **28**, 495.
15 (*a*) M. Zhou, H. Zhu, X. Wang, Y. Xu, Y. Tao, S. Hark, X. Xiao and Q. Li, *Chem. Mater.*, 2009, **22**, 64; (*b*) H. Zhu and Q. Li, *Nanoscale Res. Lett.*, 2013, **8**, 1.
16 Z. Feng, Q. Zhang, L. Lin, H. Guo, J. Zhou and Z. Lin, *Chem. Mater.*, 2010, **22**, 2705.
17 S. Joseph and P. V. Kamath, *J. Electrochem. Soc.*, 2007, **154**, E102.
18 X. Wang, H. Zhu, Y. Xu, H. Wang, Y. Tao, S. Hark, X. Xiao and Q. Li, *ACS Nano*, 2010, **4**, 3302.
19 J. Debgupta, D. B. Shinde and V. K. Pillai, *Chem. Commun.*, 2012, **48**, 3088.
20 M. Kosmulski, *J. Colloid Interface Sci.*, 2004, **275**, 214.
21 D. V. Talapin, E. V. Shevchenko, A. Kornowski, N. Gaponik, M. Haase, A. L. Rogach and H. Weller, *Adv. Mater.*, 2001, **13**, 1868.
22 (*a*) A. Ingale and K. Rustagi, *Phys. Rev. B: Condens. Matter Mater. Phys.*, 1998, **58**, 7197; (*b*) C. Trallero-Giner, *Phys. Status Solidi B*, 2004, **241**, 572.
23 D. Norris, A. L. Efros, M. Rosen and M. Bawendi, *Phys. Rev. B: Condens. Matter Mater. Phys.*, 1996, **53**, 16347.
24 (*a*) R. Venugopal, P. I. Lin, C. C. Liu and Y. T. Chen, *J. Am. Chem. Soc.*, 2005, **127**, 11262; (*b*) H. Lange, M. Artemyev, U. Woggon and C. Thomsen, *Nanotechnology*, 2009, **20**, 045705.
25 J. Kondo, *Chem. Commun.*, 1998, **3**, 357.
26 S. Chen and L.-W. Wang, *Chem. Mater.*, 2012, **24**, 3659.
27 M. Deo, S. Mujawar, O. Game, A. Yengantiwar, A. Banpurkar, S. Kulkarni, J. Jog and S. Ogale, *Nanoscale*, 2011, **3**, 4706.
28 (*a*) G. Konstantatos and E. H. Sargent, *Nat. Nanotechnol.*, 2010, **5**, 391; (*b*) L. Mandal, N. S. Chaudhari and S. Ogale, *ACS Appl. Mater. Interfaces*, 2013, **5**, 9141.

